Universality of shear-banding instability and crystallization in sheared granular fluid

MEHEBOOB ALAM[1]†, **PRIYANKA SHUKLA**[1] AND **STEFAN LUDING**[2]

[1] Engineering Mechanics Unit, Jawaharlal Nehru Center for Advanced Scientific Research

Jakkur P.O., Bangalore 560064, India.

[2]MultiScale Mechanics, Faculty of Science and Technology, University of Twente, P.O. Box 217, 7500 AE

Enschede, The Netherlands

The linear stability analysis of an uniform shear flow of granular materials is revisited using several cases of a Navier-Stokes'-level constitutive model in which we incorporate the global equation of states for pressure and thermal conductivity (which are accurate up-to the maximum packing density ν_m) and the shear viscosity is allowed to diverge at a density ν_μ ($< \nu_m$), with all other transport coefficients diverging at ν_m. It is shown that the emergence of shear-banding instabilities (for perturbations having no variation along the streamwise direction), that lead to shear-band formation along the gradient direction, depends crucially on the choice of the constitutive model. In the framework of a dense constitutive model that incorporates only collisional transport mechanism, it is shown that an accurate global equation of state for pressure or a viscosity divergence at a lower density or a stronger viscosity divergence (with other transport coefficients being given by respective Enskog values that diverge at ν_m) can induce shear-banding instabilities, even though the original dense Enskog model is stable to such shear-banding instabilities. For any constitutive model, the onset of this shear-banding instability is tied to a *universal* criterion in terms of constitutive relations for viscosity and pressure, and the sheared

† Corresponding author: Email: meheboob@jncasr.ac.in

granular flow evolves toward a state of lower "dynamic" friction, leading to the shear-induced band formation, as it cannot sustain increasing dynamic friction with increasing density to stay in the homogeneous state. A similar criterion of a lower viscosity or a lower viscous-dissipation is responsible for the shear-banding state in many complex fluids.

1. Introduction

One challenge in granular flow research is to devise appropriate hydrodynamic/continuum models to describe its macroscopic behavior. Rapid granular flows (Campbell 1990; Goldhirsch 2003) can be well modeled by an idealized system of smooth hard spheres with *inelastic* collisions. The kinetic theory of dense gases has been modified to obtain Navier-Stokes-like (NS) hydrodynamic equations, with an additional equation for the fluctuation kinetic energy of particles (i.e., granular energy) that incorporates the *dissipative*-nature of particle collisions. Such NS-order hydrodynamic models have been widely used as prototype models to gain insight into the "microscopic" understanding of various physical phenomena involved in granular flows.

The plane Couette flow has served as a prototype model problem to study the rheology (Lun *et al.* 1984; Jenkins & Richman 1985; Campbell 1990; Sela & Goldhirsch 1998; Alam & Luding 2003, 2003a; Tsai, Voth & Gollub 2003; Alam & Luding 2005; Gayen & Alam 2008) and dynamics (Hopkins & Louge 1991; McNamara 1993; Tan & Goldhirsch 1997; Alam & Nott 1997, 1998; Conway & Glasser 2004; Alam *et al.* 2005; Alam 2005, 2006; Gayen & Alam 2006; Saitoh & Hayakawa 2007) of granular materials. In the rapid shear flow, the linear stability analyses of plane Couette flow (Alam & Nott 1998; Alam 2006) showed that this flow admits different types of stationary and travelling-wave instabilities, leading to pattern formation. One such instability is the "shear-banding" instability in which the homogeneous shear flow breaks into alternating dense and dilute regions of particles along the gradient direction. This is

dubbed "shear-banding" instability since the "nonlinear" saturation of this instability (Alam & Nott 1998; Alam *et al.* 2005; Shukla & Alam 2008) leads to alternate layers of dense and dilute particle-bands in which the shear-rate is high/low in dilute/dense regions, respectively, leading to "shear-localization" (Varnik *et al.* 2003). This is reminiscent of shear-band formation in shear-cell experiments (Savage & Sayed 1984; Losert *et al.* 2000; Mueth *et al.* 2000; Alam & Luding 2003; Tsai, Voth & Gollub 2003): *when a dense granular material is sheared the shearing is confined within a few particle-layers (i.e., a shear-band) and the rest of the material remains unsheared*, leading to the two-phase flows of dense and dilute regions. Previous works (Alam & Nott 1998; Alam *et al.* 2005) showed that the kinetic-theory-based hydrodynamic models are able to predict the co-existence of dilute and dense regimes of such shear-banding patterns.

The above problem has recently been reanalyzed (Khain & Meerson 2006), with reference to shear-band formation, with a constitutive model which is likely to be valid in the dense limit. These authors showed that their 'dense' constitutive model does not admit shear-banding instabilities of Alam & Nott (1998); however, a single modification that the shear viscosity diverges at a density lower than other transport coefficients resulted in the appearance of two-phase-type solutions of dilute and dense flows that are reminiscent of shear-banding instabilities. That the viscosity diverges stronger/faster than other transport coefficient has also been incorporated previously in a constitutive model by Losert *et al.* (2000) that yields a satisfactory prediction for shear-bands in an experimental Couette flow in three-dimensions.

We revisit this problem to understand the influence of different Navier-Stokes'-order constitutive models (as detailed in §2) on the shear-banding instabilities in granular plane Couette flow. More specifically, we will pinpoint how the effects of various models, some of them involving the global equation of state and the viscosity divergence (at a density lower than the maximum packing), change the shear-banding instabilities predicted by Alam & Nott (1998). For the sake of a systematic overview, we will also discuss about the instability results based on special lim-

iting cases of these models. One important finding is that a global equation of state (*without viscosity divergence at a lower density*) leads to a shear-banding instability in the framework of a "dense" model that incorporates only collisional transport mechanism. Even with the local equation of state, if we use a constitutive relation for viscosity that has a stronger divergence (at the same maximum packing density) than other transport coefficients, we recover shear-banding instabilities in the framework of the dense-model of Haff (1983). This brings us to a *crossroad*: is there any connection among the results of Alam & Nott, Khain & Meerson, and the present work? Is there any *universal* criterion for the onset of the shear-banding instability in granular shear flow? Such an universality for the shear-banding instability indeed exists, solely in terms of the constitutive relations, as we show in this paper. Possible connections of the present criterion of a lower dynamic friction for the shear-banding state to explain the onset of shear-banding in many complex fluids as well as in an elastic hard-sphere fluid are discussed.

2. Balance equations and constitutive model

We use a Navier-Stokes-level hydrodynamic model for which we need balance equations for mass, momentum and granular temperature:

$$\left(\frac{\partial}{\partial t} + \mathbf{u} \cdot \boldsymbol{\nabla}\right)\varrho = -\varrho \boldsymbol{\nabla} \cdot \mathbf{u} \tag{2.1}$$

$$\varrho\left(\frac{\partial}{\partial t} + \mathbf{u} \cdot \boldsymbol{\nabla}\right)\mathbf{u} = -\boldsymbol{\nabla} \cdot \mathbf{P} \tag{2.2}$$

$$\frac{\dim}{2}\varrho\left(\frac{\partial}{\partial t} + \mathbf{u} \cdot \boldsymbol{\nabla}\right)T = -\boldsymbol{\nabla} \cdot \mathbf{q} - \mathbf{P} : \boldsymbol{\nabla}\mathbf{u} - \mathcal{D}. \tag{2.3}$$

Here $\varrho = mn = \rho_p \nu$ is the mass-density, m the particle mass, n the number density, ρ_p the material density and ν the area/volume fraction of particles; $\mathbf{u}$ is the coarse-grained velocity-field and T is the granular temperature of the fluid. Note that the granular temperature, $T = \langle C^2 / \dim \rangle$, is defined as the mean-square fluctuation velocity, with $\mathbf{C} = (\mathbf{c} - \mathbf{u})$ being the peculiar velocity of particles and $\mathbf{c}$ the instantaneous particle velocity; $\dim$ is the dimensionality

of the system and here onward we focus on the two-dimensional ($\dim = 2$) system of an inelastic

"hard-disk" fluid. The flux terms are the stress tensor, $\mathbf{P}$, and the granular heat flux, $\mathbf{q}$; $\mathcal{D}$ is the

rate of dissipation of granular energy per unit volume– for these three terms we need appropriate

constitutive relations which are detailed below.

2.1. *General form of Newtonian constitutive model: Model-A*

The standard Newtonian form of the stress tensor and the Fourier law of heat flux are:

$$\mathbf{P} = (p - \zeta \boldsymbol{\nabla} \cdot \mathbf{u})\mathbf{I} - 2\mu \mathbf{S}, \tag{2.4}$$

$$\mathbf{q} = -\kappa \boldsymbol{\nabla} T, \tag{2.5}$$

where $\mathbf{I}$ is the identity tensor and $\mathbf{S}$ the deviator of the deformation rate tensor. Here p, μ, ζ

and κ are pressure, shear viscosity, bulk viscosity and thermal conductivity of the granular fluid,

respectively.

Focussing on the nearly elastic limit ($e \to 1$) of an inelastic hard-disk (of diameter d) fluid,

the constitutive expressions for p, μ, ζ, κ and $\mathcal{D}$ are given by

$$
\begin{aligned}
p(\nu, T) &= \rho_p f_1(\nu)T, & \mu(\nu, T) &= \rho_p d f_2(\nu)\sqrt{T}, \\
\zeta(\nu, T) &= \rho_p d f_3(\nu)\sqrt{T}, & \kappa(\nu, T) &= \rho_p d f_4(\nu)\sqrt{T}, \\
\mathcal{D}(\nu, T) &= \tfrac{\rho_p}{d} f_5(\nu, e)T^{3/2},
\end{aligned}
\tag{2.6}
$$

where f_1–f_5 are non-dimensional functions of the particle area fraction ν (Gass 1971; Jenkins &

Richman 1985):

$$f_1(\nu) = \nu + 2\nu^2 \chi, \tag{2.7}$$

$$f_2(\nu) = \frac{\sqrt{\pi}}{8\chi} + \frac{\sqrt{\pi}}{4}\nu + \frac{\sqrt{\pi}}{8}\left(1 + \frac{8}{\pi}\right)\nu^2 \chi, \tag{2.8}$$

$$f_3(\nu) = \frac{2}{\sqrt{\pi}}\nu^2 \chi, \tag{2.9}$$

$$f_4(\nu) = \frac{\sqrt{\pi}}{2\chi} + \frac{3\sqrt{\pi}}{2}\nu + \sqrt{\pi}\left(\frac{2}{\pi} + \frac{9}{8}\right)\nu^2 \chi, \tag{2.10}$$

$$f_5(\nu, e) = \frac{4}{\sqrt{\pi}}(1 - e^2)\nu^2 \chi. \tag{2.11}$$

These constitutive expressions give good predictions for transport coefficients of nearly elastic

granular fluid up-to a density of $\nu \approx 0.55$ (see, figure 2 of Alam & Luding 2003a). In the above

expressions, $\chi(\nu)$ is the contact radial distribution function which is taken to be of the following

form (Henderson 1975)

$$\chi(\nu) = \frac{1 - 7\nu/16}{(1 - \nu/\nu_m)^2},\tag{2.12}$$

that diverges at some finite density $\nu = \nu_m$. For the ideal case of point particles (i.e. in one

dimension, Torquato 1995), we have $\nu_m = 1$ which is unrealistic for macroscopic grains at very

high densities; there are two other choices for this diverging density: the random close packing

density $\nu_r = \nu_m = 0.82$ or the maximum packing density $\nu_m = \pi/2\sqrt{3} \approx 0.906$ in two-

dimensions (Torquato 1995); up-to some moderate density ($\nu \sim 0.5$), there is no difference in

the value of $\chi(\nu)$ for any choice of $\nu_m = 1$ or 0.906 or 0.82. The range of validity of different

variants of model radial distribution functions is discussed in an upcoming paper (Luding 2008).

We shall denote the above constitutive model (2.6–2.11), with the contact radial distribution

function being given by (2.12), as "model-A". Since the stability results do not differ qualitatively

with either choice of the numerical value for ν_m ($= 0.82$ or 0.906 or 1), we will present all results

with $\nu_m = \pi/2\sqrt{3}$ in (2.12) (except in figure 12d, see §5.2).

Now we consider the dilute and dense limits of model-A. It should be noted that each transport

coefficient has contributions from the 'kinetic' and 'collisional' modes of transport: while the

former is dominant in the Boltzmann limit ($\nu \to 0$), the latter is dominant in the dense limit ($\nu \to$

ν_m). For example, the pressure can be decomposed into its kinetic and collisional contributions:

$$p = p^k + p^c = \rho_p(f_1^k + f_1^c)T.\tag{2.13}$$

To obtain the constitutive expressions for the dilute and dense regimes, one has to take the ap-

propriate limit of all functions f_1–f_4:

$$
\begin{aligned}
f_1 &= f_1^k + f_1^c, \quad f_2 = f_2^k + f_2^c, \\
f_3 &= f_3^k + f_3^c, \quad f_4 = f_4^k + f_4^c.
\end{aligned}
\tag{2.14}
$$

Based on this decomposition, we have the following two limiting cases of model-A.

2.1.1. *Dilute limit: Model A_0*

For this dilute ($\nu \to 0$) model, $\chi(\nu) \to 1$ and the constitutive expressions are assumed to contain contributions only from the kinetic mode of transport:

$$
\begin{aligned}
f_1 \equiv f_1^k(\nu) &= \nu, & f_2 \equiv f_2^k(\nu) &= \tfrac{\sqrt{\pi}}{8} + \tfrac{\sqrt{\pi}}{4}\nu, \\
f_3 \equiv f_3^k(\nu) &= 0, & f_4 \equiv f_4^k(\nu) &= \tfrac{\sqrt{\pi}}{2} + \tfrac{3\sqrt{\pi}}{2}\nu, \\
f_5 \equiv f_5(\nu \to 0) &= \tfrac{4}{\sqrt{\pi}}(1 - e^2)\nu^2.
\end{aligned}
\tag{2.15}
$$

We shall call this "model A_0". Note that f_5 has only the leading-order collisional contribution, since no energy is dissipated in kinetic (free-flow) motion.

2.1.2. *Dense limit: Model A_d*

For this *dense* model, the constitutive expressions are assumed to contain contributions only from collisional mode of transport:

$$
\begin{aligned}
f_1 \equiv f_1^c(\nu) &= 2\nu^2\chi, & f_2 \equiv f_2^c(\nu) &= \tfrac{\sqrt{\pi}}{8}\left(1 + \tfrac{8}{\pi}\right)\nu^2\chi, \\
f_3 \equiv f_3^c(\nu) &= \tfrac{2}{\sqrt{\pi}}\nu^2\chi, & f_4 \equiv f_4^c(\nu) &= \sqrt{\pi}\left(\tfrac{2}{\pi} + \tfrac{9}{8}\right)\nu^2\chi, \\
f_5 \equiv f_5(\nu, e) &= \tfrac{4}{\sqrt{\pi}}(1 - e^2)\nu^2\chi.
\end{aligned}
\tag{2.16}
$$

We shall call this "model A_d" which is nothing but Haff's model (1983).

2.2. *Model B: global equation of state (EOS)*

In two-dimensions, a global equation of state for pressure has recently been proposed by Luding (2001):

$$
p/\rho_p T \equiv f_1(\nu) = \nu + \nu\left(P_4 + m(\nu)\left[P_{dense} - P_4\right]\right), \quad \forall \quad 0 \leqslant \nu \leqslant \nu_m = \frac{\pi}{2\sqrt{3}}, \tag{2.17}
$$

where

$$
\begin{aligned}
P_4 &= 2\nu\chi_4, \\
\chi_4(\nu) &= \frac{1-7\nu/16}{(1-\nu)^2} - \frac{\nu^3}{128(1-\nu)^4}, \\
P_{dense} &= \frac{2\nu_m h_3(\nu_m - \nu)}{(\nu_m - \nu)} - 1, \\
h_3(\nu_m - \nu) &= 1 - 0.04(\nu_m - \nu) + 3.25(\nu_m - \nu)^3, \\
m(\nu) &= \left[1 + \exp(-(\nu - \nu_f)/m_0)\right]^{-1}.
\end{aligned}
\tag{2.18}
$$

Here ν_f is the freezing point density, and $m(\nu)$ is a merging function that selects P_4 for $\nu << \nu_f$ and P_{dense} for $\nu >> \nu_f$; the value of m_0 is taken to be 0.012 along with a freezing density of $\nu_f = 0.7$. It should be noted that the above functional form of $f_1(\nu)$, (2.17), is a monotonically increasing function of ν, and it has been verified (Luding 2001, 2002; Garcia-Rojo, Luding & Brey 2006) from molecular dynamics simulations of elastic hard-disk systems that the numerical values for different constants in (2.18) are accurate (within much less than 1% except around ν_f) up-to the maximum packing density.

Rewriting equation (2.17) as

$$
f_1(\nu) = \nu + 2\nu^2\chi^p(\nu), \tag{2.19}
$$

we can define an "effective" contact radial distribution function for pressure:

$$
\begin{aligned}
\chi^p(\nu) &= \frac{1}{2\nu}\left(P_4 + m(\nu)\left[P_{dense} - P_4\right]\right), \\
&= \chi_4 + m(\nu)\left[\frac{h_3(\nu_m - \nu)}{\nu(1 - \nu/\nu_m)} - \frac{1}{2\nu} - \chi_4\right], \quad \text{with} \quad \nu_m = \frac{\pi}{2\sqrt{3}}. \tag{2.20}
\end{aligned}
$$

It should be noted here that this functional form of $\chi^p(\nu)$ has been verified by molecular dynamics simulations of plane shear flow of frictional inelastic disks (Volfson, Tsimring & Aranson 2003). In particular, they found that the simulation data on $G(\nu) = \nu\chi^p(\nu)$ agree with the predictions of (2.20), however, its divergence appears to occur at the random close packing limit in two-dimensions ($\nu_m = \nu_r = 0.82$).

Similar to pressure, a global equation for thermal conductivity has been suggested by Garcia-

Rojo *et al.* (2006) which is also accurate up-to the maximum packing density. More specifically, the non-dimensional function of density for thermal conductivity (equation (2.10)) is replaced by

$$f_4(\nu) = \frac{\sqrt{\pi}}{2\chi^\kappa(\nu)} + \frac{3\sqrt{\pi}}{2}\nu + \sqrt{\pi}\left(\frac{2}{\pi} + \frac{9}{8}\right)\nu^2\chi^\kappa(\nu) \qquad (2.21)$$

where $\chi^\kappa(\nu)$ is the "effective" contact radial distribution function for thermal conductivity:

$$\chi^\kappa(\nu) = \chi(\nu, \nu_m = 1) + m(\nu)\left[\frac{h_3(\nu_m - \nu)}{\nu(1 - \nu/\nu_m)} - \frac{1}{2\nu} - \chi(\nu, \nu_m = 1)\right], \qquad (2.22)$$

with $\chi(\nu, \nu_m = 1)$ being obtained from (2.12) by putting $\nu_m = 1$.

The model-A with the above global equation of state for pressure and the global equation for thermal conductivity is called "model-B". Note that the dilute limit of model-B is the same as that of model-A, however, the dense limits of both models are different in the choice of the equation of state and thermal conductivity.

Now we identify two subsets of model-B: "model-B^p" and "model-B^κ" where the former is model-B with a global equation of state for pressure (2.17) only and the latter is model-B with a global equation for thermal conductivity (2.21) only. As clarified in the previous paragraph, the remaining transport coefficients of model-B are same as in model-A.

2.3. *Model-C: viscosity divergence*

Here we consider a variant of model-A which incorporates another ingredient in the constitutive model: *the shear viscosity diverges at a density lower than other transport coefficients* (Garcia-Rojo *et al.* 2006). This can be incorporated in the corresponding dimensionless function for the shear viscosity (2.8):

$$f_2^\mu(\nu) = f_2(\nu)\left(1 + \frac{0.037}{\nu_\mu - \nu}\right), \qquad (2.23)$$

which diverges at a density, $\nu = \nu_\mu < \nu_m$, that is lower than the close packing density. The first term on the right-hand-side is the standard Enskog term (2.8) and the second term incorporates a correction due to the viscosity divergence. For all results shown here, we use $\nu_\mu = 0.71$ which

was observed for the unsheared case (Garcia-Rojo *et al.* 2006); note, however, that the precise

density at which viscosity diverges in a shear flow can be larger than 0.71 (see figure 6 of Alam

& Luding 2003).

The model with all transport coefficients as in model-A but with its viscosity divergence being

at a lower density is termed as "model-C". Similar to model-A, we can recover the dilute and

dense limits of model-C, by separating the kinetic and collisional contributions to each transport

coefficient. The dense limit of model-C is, however, reached at $\nu = \nu_\mu$ due to the viscosity

divergence.

2.4. *Model-D: Global equation of state and viscosity divergence*

This is the most general model in which we incorporate: (1) the global equation of state for

pressure (2.17), (2) the global equation for thermal conductivity (2.21), and (3) the viscosity

divergence (2.23). The other transport coefficients of model-D are same as in model-A.

3. Plane shear and linear stability

Let us consider the plane shear flow of granular materials between two walls that are separated

by a distance $\tilde{H}$: the top wall is moving to the right with a velocity $U_w/2$ and the bottom wall

is moving to the left with the same velocity. We impose no-slip and zero heat-flux boundary

conditions at both walls:

$$\mathbf{u} = \pm U_w/2 \quad \text{and} \quad \mathbf{q} = 0 \quad \text{at} \quad y = \pm \tilde{H}/2. \tag{3.1}$$

The equations of motion for the steady and fully developed shear flow admit the following

solution:

$$\mathbf{u} = [u(y), v(y)] = [(U_w/\tilde{H})y, 0], \quad \nu(y) = const. = \overline{\nu}, \quad T = d^2 \left(\frac{\mathrm{d}u}{\mathrm{d}y}\right)^2 \frac{f_2(\nu)}{f_5(\nu)}. \tag{3.2}$$

The shear rate, $\mathrm{d}u/\mathrm{d}y = U_w/\tilde{H}$, is uniform (constant) across the Couette gap, and this solution

will henceforth be called *uniform shear solution*. Note that if viscosity diverges at $\nu = \nu_\mu$, there

is *no* uniform shear solution for $\nu > \nu_\mu$, i.e. the uniform shear flow is possible only for densities

$0 < \nu < \nu_\mu$.

We have non-dimensionalized all quantities by using $\tilde{H}$, $\tilde{H}/U_w$ and U_w as the reference

length, time and velocity scales, respectively. The explicit forms of dimensionless balance equa-

tions as well as the dimensionless transport coefficients are written down in Appendix A. There

are three dimensionless control parameters to characterize our problem: the scaled Couette gap

$H = \tilde{H}/d$, the mean density (area fraction) $\nu = \overline{\nu}$ and the restitution coefficient e. Here onwards,

all quantities are expressed in dimensionless form.

3.1. *Linear stability*

The stability analysis of the plane shear flow has been thoroughly investigated (Alam & Nott

1998; Alam 2005, 2006; Alam *et al.* 2005) using the constitutive models of class A for which

all transport coefficients diverge at the maximum packing fraction $\nu \to \nu_m$, as outlined in §2.1.

The same analysis is carried out here for a specific type of perturbations that are *invariant* along

the streamwise/flow (x) direction, having variations along the gradient (y) direction only. This

implies that the x-derivatives of all quantities are set to zero $(\partial/\partial x(\cdot) = 0)$ in the governing

equations. The analysis being identical with that of Alam and Nott (1998), we refer the readers

to that article for mathematical details.

Consider the stability of the uniform shear solution (3.2) against perturbations that have spatial

variations along the y-direction only, e.g. the density field can be written as $\nu(y,t) = \nu + \nu'(y,t)$,

with the assumption of small-amplitude perturbations, $|\nu'(y,t)/\nu| << 1$, for the linear analysis.

Linearizing around the uniform shear solution, we obtain a set of partial differential equations:

$$\frac{\partial X}{\partial t} = \mathcal{L}X, \quad \text{with} \quad \mathcal{B}X \equiv \left(1, 1, \frac{\mathrm{d}}{\mathrm{d}y}\right) \cdot (u', v', T') = 0, \tag{3.3}$$

where $X = (\nu', u', v', T')$ is the vector of perturbation fields, $\mathcal{L}$ is the linear stability operator

and $\mathcal{B}$ denotes the boundary operator (i.e., zero slip, zero penetration and zero heat flux). Assum-

ing exponential solutions in time $X(y,t) = \hat{X}(y)\exp(\omega t)$, we obtain a differential-eigenvalue

problem:

$$\omega\hat{X} = \mathcal{L}\left(\frac{\mathrm{d}^2}{\mathrm{d}y^2}, \frac{\mathrm{d}}{\mathrm{d}y}, \ldots\right)\hat{X}, \quad \text{with} \quad \mathcal{B}\hat{X} = 0, \tag{3.4}$$

where $\hat{X}(y) = (\hat{\nu}, \hat{u}, \hat{v}, \hat{T})(y)$ is the unknown disturbance vector that depends on y. Here,

$\omega = \omega_r + i\omega_i$ is the complex frequency whose real part ω_r denotes the growth/decay rate of

perturbations and the imaginary part ω_i is its frequency which characterizes the propagating

($\omega_i \neq 0$) or stationary ($\omega_i = 0$) nature of the disturbance. The flow is stable or unstable if $\omega_r < 0$

or $\omega_r > 0$, respectively.

3.2. *Analytical solution: dispersion relation and its roots*

Before presenting numerical stability results (§4), we recall that the above set of ordinary differ-

ential equations (3.4) admits an analytical solution (Alam & Nott 1998):

$$(\hat{\nu}(y), \hat{T}(y)) = (\nu_1, T_1)\cos k_n(y \pm 1/2) \tag{3.5}$$

$$(\hat{u}(y), \hat{v}(y)) = (u_1, v_1)\sin k_n(y \pm 1/2), \tag{3.6}$$

where $k_n = n\pi$ is the 'discrete' wavenumber along y, with $n = 1, 2, \ldots$ being the mode number

that tells us the number of zero-crossing of the density/temperature eigenfunctions along $y \in$

$(-1/2, 1/2)$. With this, equation (3.4) boils down to an algebraic eigenvalue problem:

$$\mathcal{A}X_1 = \omega X_1, \tag{3.7}$$

where $X_1 = (\nu_1, u_1, v_1, T_1)$ and $\mathcal{A}$ is a 4×4 matrix. This leads to a fourth-order dispersion

relation in ω:

$$\omega^4 + a_3\omega^3 + a_2\omega^2 + a_1\omega + a_0 = 0, \tag{3.8}$$

with coefficients

$$\begin{aligned} a_0 &= \tfrac{1}{H^4}a_{04} + \tfrac{1}{H^6}a_{06}, \quad a_1 = \tfrac{1}{H^2}a_{12} + \tfrac{1}{H^4}a_{14} + \tfrac{1}{H^6}a_{16}, \\ a_2 &= \tfrac{1}{H^2}a_{22} + \tfrac{1}{H^4}a_{24}, \quad a_3 = a_{30} + \tfrac{1}{H^2}a_{32}. \end{aligned} \tag{3.9}$$

Here a_{ij}'s are real functions of density (ν), temperature (T), and the restitution coefficient (e) whose explicit forms are written down in Appendix B.

Out of four roots of (3.8), two roots are real and the other two form a complex-conjugate pair. It is possible to obtain an approximate analytical solution for these four roots using the standard asymptotic expansion for *large* Couette gaps ($H \equiv \tilde{H}/d$), with the corresponding small parameter being H^{-1}. The real roots have the approximations for large H:

$$\omega^{(1)} = -\frac{1}{H^2}\left(\frac{a_{04}}{a_{12}}\right) + O\left(H^{-4}\right), \tag{3.10}$$

$$\omega^{(2)} = \omega_0^{(2)} + \frac{1}{H^2}\frac{\left[a_{12} + a_{22}\omega_0^{(2)} + a_{32}\omega_0^{(2)^2}\right]}{\omega_0^{(2)}\left(3a_{30} + 4\omega_0^{(2)}\right)} + O\left(H^{-4}\right), \tag{3.11}$$

where

$$\omega_0^{(2)} = -\frac{1}{\nu}f_5 T^{1/2} < 0. \tag{3.12}$$

The real and imaginary parts of the conjugate pair,

$$\omega^{(3,4)} = \omega_r^{(3,4)} \pm \mathrm{i}\,\omega_i^{(3,4)}, \tag{3.13}$$

have the asymptotic approximations for large H:

$$\omega_r^{(3,4)} = \frac{1}{H^2}\left[\frac{a_{04} + \left(\frac{a_{12}^2}{a_{30}^2}\right) - \left(\frac{a_{12}a_{22}}{a_{30}}\right)}{2a_{12}}\right] + O\left(H^{-4}\right), \tag{3.14}$$

$$(\omega_i^{(3,4)})^2 = \frac{1}{H^2}\left(\frac{a_{12}}{a_{30}}\right) + O\left(H^{-4}\right). \tag{3.15}$$

For full models (i.e., A, B, C and D), it can be verified that $\omega_r^{(3,4)}$ is always negative, making the first real root $\omega^{(1)}$, given by (3.10), the least-stable mode. However, for the dense models (i.e., A_d, B_d, C_d and D_d), $\omega_r^{(3,4)}$ could be positive, making the travelling waves, given by (3.13), the least-stable mode at low densities. These predictions have been verified against numerical values obtained from spectral method as discussed in §4.

4. Stability results: comparison among different models

For results in this section, the differential eigenvalue problem (3.4) has been discretized using the Chebyshev spectral method (Alam & Nott 1998) and the resultant algebraic eigenvalue problem has been solved using the QR-algorithm of the Matlab-software. The degree of the Chebyshev polynomial was set to 20 which was found to yield accurate eigenvalues. In principle, we could solve (3.8) to obtain eigenvalues, but it provides eigenvalues only for a given mode number $n = 1, 2, \ldots$ in one shot; therefore, one has to solve (3.8) for several n to determine the growth rate of the most unstable mode. The advantage of the numerical solution of (3.4) is that it provides all leading eigenvalues in one shot.

4.1. *Results for model-A and its dilute and dense limits*

As mentioned before, the stability analysis of the uniform shear flow with a 3D-variant (i.e. for spheres) of model-A has been performed before (Alam & Nott 1998; Alam 2005, 2006; Alam *et al.* 2005). Even though the results for our 2D-model are similar to those for the 3D-model, we show a few representative results for this constitutive model for the sake of a complete, systematic study and for comparison with other models; note that the results for model-A_0 and model-A_d are new.

The phase diagram, separating the zones of stability and instability, in the (ν, H)-plane is shown in figure 1 for model-A. The flow is *unstable* inside the neutral contour, denoted by '0', and *stable* outside; a few positive growth-rate contours are also displayed. For the same parameter set, from the respective contours of the frequency, ω_i, in the (ν, H)-plane it has been verified that these instabilities are *stationary*, i.e., $\omega_i = 0$. It is seen that there is a minimum value of the Couette gap ($H = H_{cr}$) and a minimum density ($\nu = \nu_{cr}$) below which the flow remains stable. With increasing value of e, the neutral contour shifts towards the right, i.e., H_{cr} increases and hence the flow becomes more stable with increasing e. We shall discuss the dependence of e on the shear-banding instability and the related instability length scale in §5.2.
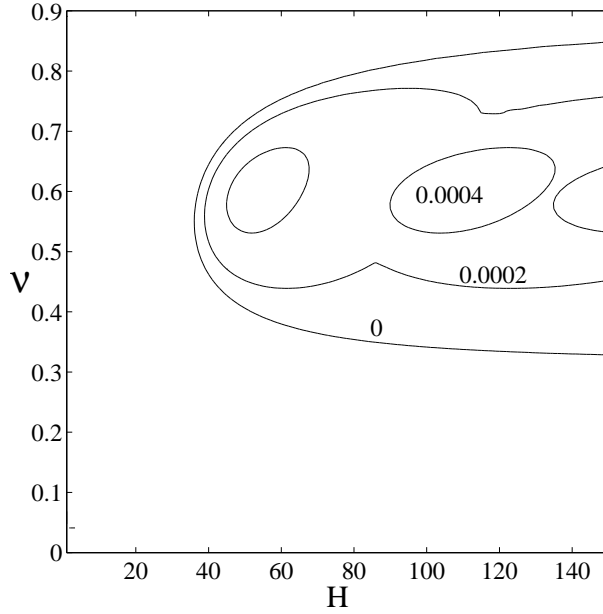
FIGURE 1. Phase diagram, showing the positive growth-rate contours, for model-A: $e = 0.9$, $\nu_m = \pi/2\sqrt{3}$. The flow is unstable inside the neutral contour, denoted by '0', and stable outside.
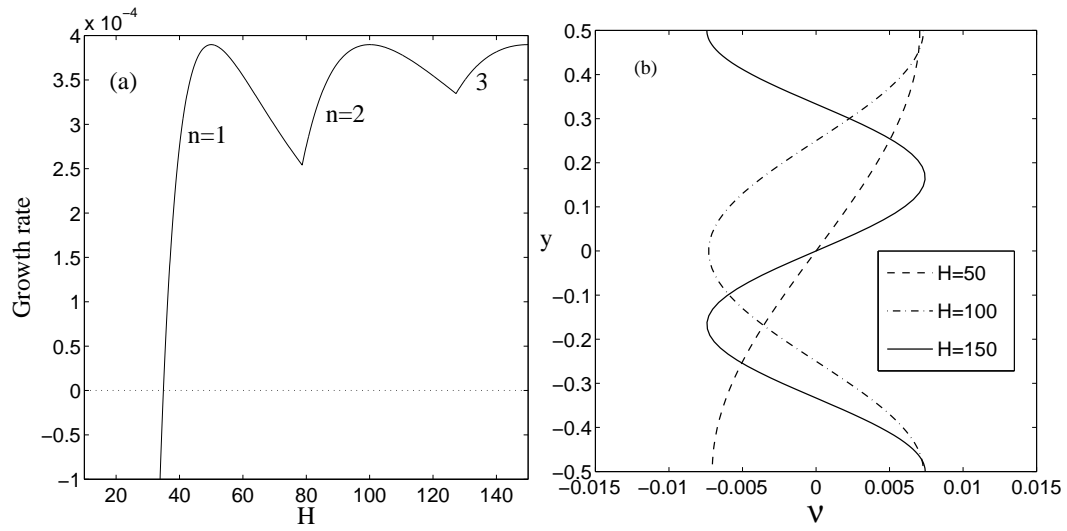

FIGURE 2. (a) Variation of the growth rate of the least stable mode with H for $\nu = 0.5$ and $e = 0.9$. (b) Density eigenfunctions, $\hat{\nu}(y)$, of the least stable mode at $H = 50$, 100 and 150.
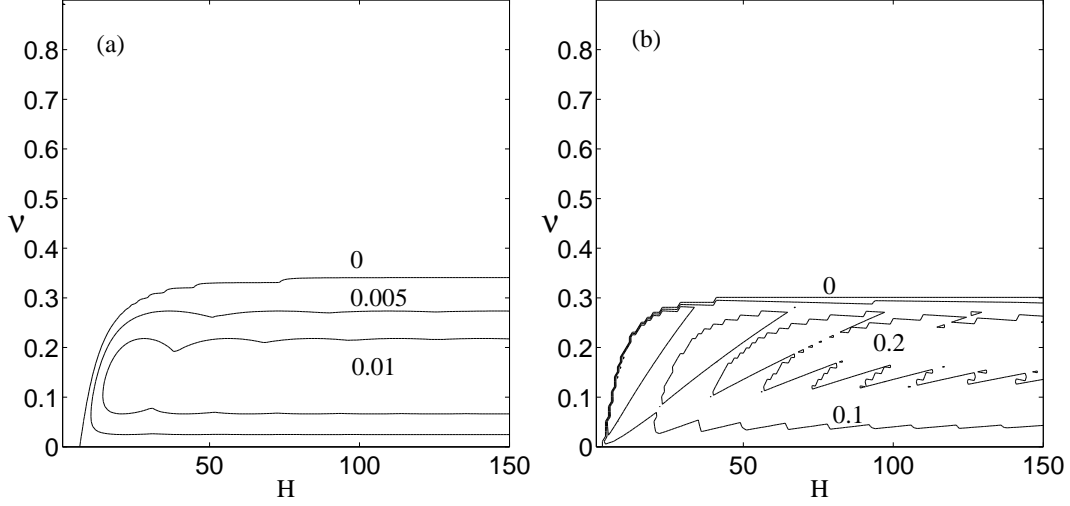
FIGURE 3. (*a*) Phase diagram, showing the positive growth-rate contours, for model-A_d (i.e., the dense limit of model-A): $e = 0.9$, $\nu_m = \pi/2\sqrt{3}$. (*b*) Contours of frequency, indicating that the instability in panel *a* is due to travelling waves.

Figure 2(*a*) shows the variation of the growth rate of the least stable mode, $\omega_r^l = \max \omega_r$, with Couette gap for $\nu = 0.5$, with other parameters as in figure 1. The kinks on the growth-rate curve correspond to crossing of modes $n = 1, 2, 3, \cdots$. This can be verified from figure 2(*b*) which displays density eigenfunctions for three values of Couette gaps $H = 50$, 100 and 150. The density eigenfunction at $H = 50$ corresponds to the mode $n = 1$ (i.e. $\hat{\nu} \sim \cos(\pi(y \pm 1/2)) = \sin(\pi y)$, see equation (3.5)), the other two at $H = 100, 150$ correspond to modes $n = 2, 3$ (i.e., $\hat{\nu} \sim \cos(2\pi y)$ and $\sin(3\pi y)$, respectively). In fact, there is an infinite hierarchy of such modes as $H \to \infty$ which has been discussed before (Alam & Nott 1998; Alam *et al.* 2005).

For the dilute limit of model-A (i.e., model-A_0), there are *stationary* instabilities at finite densities ($\nu > 0$), and the stability diagram (not shown for brevity) in the (H, ν)-plane looks similar to that for model-A (figure 1), but the range of H over which the flow is unstable is much larger. As expected, both model-A and model-A_0 predict that the flow is stable in the Boltzmann limit ($\nu \to 0$).

Figure 3(*a*) shows the analogue of figure 1 for model-A_d for which the constitutive relations
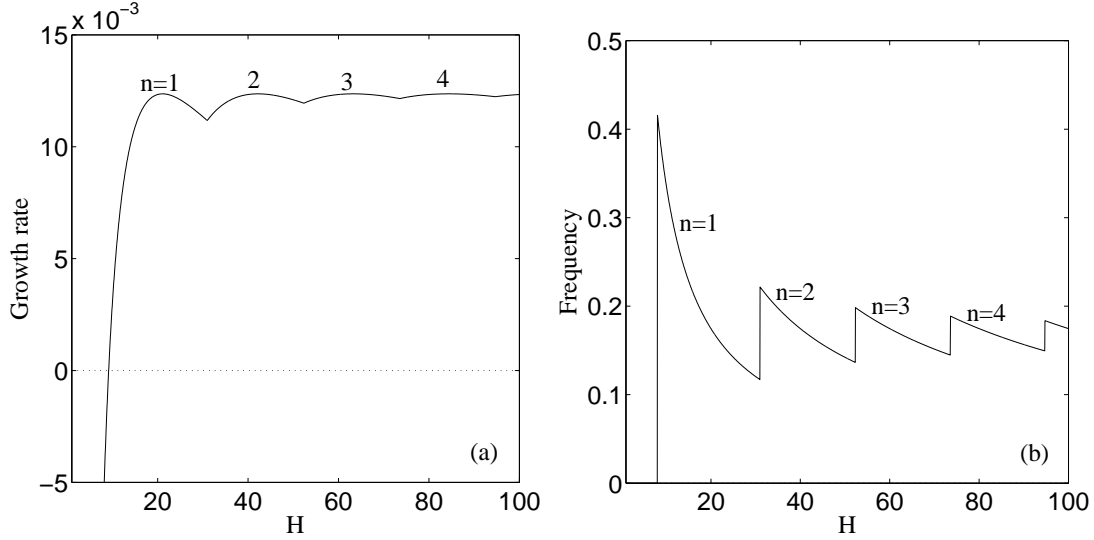
FIGURE 4. Variations of (a) the growth rate and (b) the frequency of the least stable mode with H for $\nu = 0.1$ and $e = 0.9$. Other parameters as in figure 3.

are expected to be valid in the dense limit (since the constitutive relations contain the collisional part only, §2.1.2); figure 3(b) shows the contours of frequency (corresponding to the least-stable mode) in the (H, ν)-plane. The flow is unstable to *travelling-wave* instabilities inside the neutral contour. For this dense model, the crossings of different instability modes ($n = 1, 2, \cdots$) with increasing Couette gap H and their frequency variations can be ascertained from figure 4. From a comparison between figures 1 and 3, the following differences are noted:

(1) Model-A_d predicts that the flow is stable in the dense limit which is in contrast to the prediction of the full model (i.e., model-A) for which the dense flow is unstable. This is a surprising result since the kinetic contribution to transport coefficients is small in the dense limit, and hence both model-A and model-A_d are expected to yield similar results.

(2) There is a travelling-wave (TW) instability at low densities ($\nu < 0.3$) for model-A_d which is absent in model-A. Since model-A_d is devoid of the kinetic modes of momentum transfer and hence not applicable at low densities, we call the TW-modes in figure 3(a) as "anomalous"
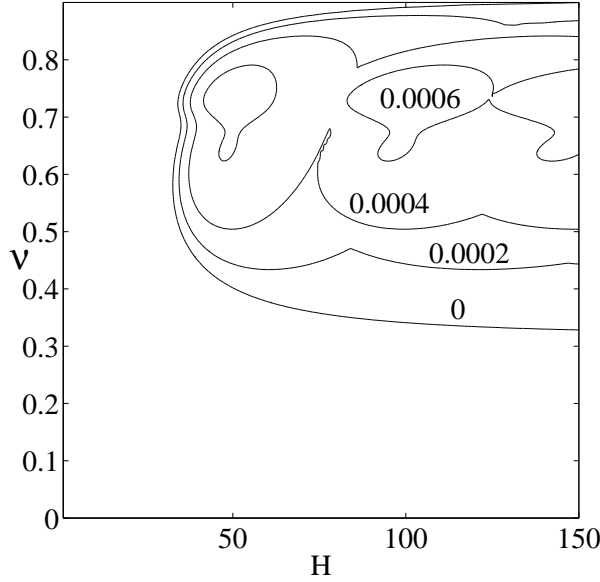
FIGURE 5. Phase diagram, showing the positive growth-rate contours, for model-B^κ with a global equation for thermal conductivity: $e = 0.9$, $\nu_m = \pi/2\sqrt{3}$, $\nu_f = 0.7$.

modes and they vanish when both kinetic and collisional effects are incorporated as in the full model-A.

One conclusion that can be drawn from the results of three variants of model-A is that the choice of the constitutive model is crucial for the prediction of shear-banding instability. We shall come back to discuss this point in § 5.

4.2. *Results for model-B: influence of global equation of state*

Figure 5 shows a phase-diagram in the (H, ν)-plane for model B^κ; the flow is unstable inside the neutral contour and stable outside. Recall that this model is the same as model-A for $\nu < \nu_f$, with the only difference being that we use a global equation for thermal conductivity which is valid up-to the maximum packing density (equation 2.21). This instability is stationary and the other features of stability diagrams remain the same (as those in figure 1 for the standard model-A), but there is a dip on the neutral contour at the freezing density $\nu = \nu_f$. For its dense counterpart, the model-B_d^κ does not predict any instability at large densities but has travelling-wave instability at
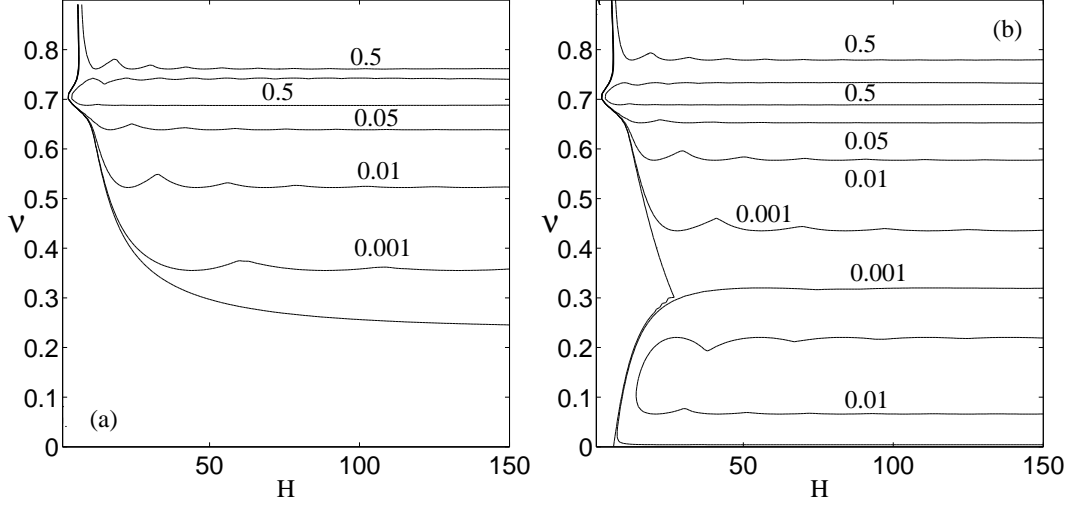
FIGURE 6. Phase diagram, showing the positive growth-rate contours, for model-B^p with a global equation for pressure: $e = 0.9$, $\nu_m = \pi/2\sqrt{3}$, $\nu_f = 0.7$. (a) Full model; (b) dense limit.

low densities (the corresponding stability diagram looks similar to that in figure 3(a) for model-A_d and hence is not shown).

When a global equation of state for pressure is incorporated (i.e., model-B^p, see §2.2), the phase-diagram in the (H, ν)-plane looks markedly different, especially at $\nu > \nu_f$, as seen in figures 6(a) and 6(b). (Recall that the model-B^p is same as model-A, except that we use a global equation of state for pressure, equation (2.17).) In figure 6(b), the neutral stability contour contains a kink at $\nu \approx 0.3$ and there are two instability-lobes: the lower instability lobe is due to *travelling-waves* and the upper-one is due to *stationary-waves*. (Similar to model-A_d, the low density TW instability in figure 6(b) is dubbed "anomalous" since model-B_d is not valid at low densities.) It is interesting to note in figure 6(b) that for the dense limit of model-B^p (i.e., model-B_d^p) the flow remains unstable to the "stationary" shear-banding instability up-to the maximum packing density. This observation is in contrast to the predictions of model-A_d (figure 3a) and model-B_d^κ. Therefore, we conclude that *within the framework of a dense model the global equation of state for pressure induces shear-banding instabilities at large densities.*

When both the global equations for pressure and thermal conductivity are incorporated, the
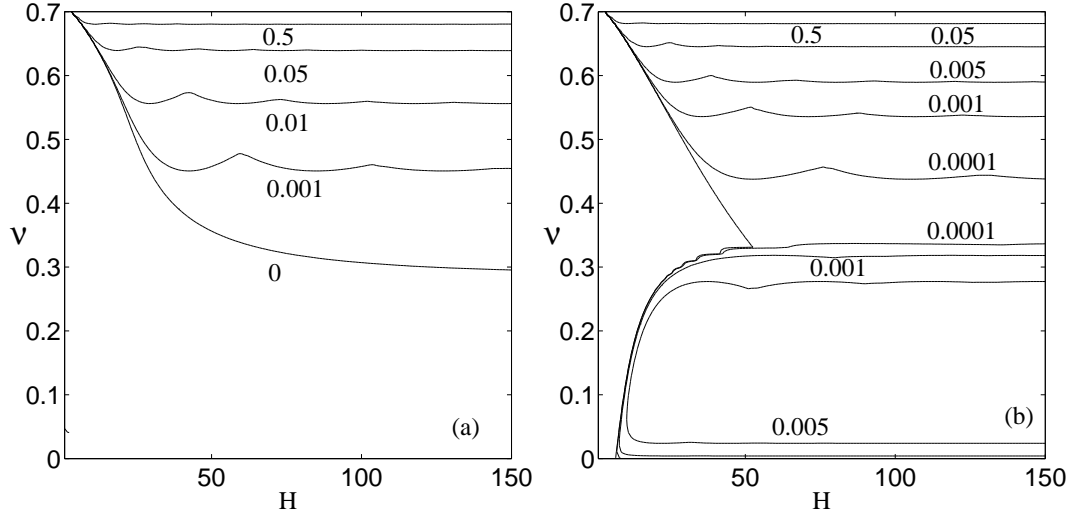
FIGURE 7. Phase diagram for model-C with viscosity divergence: $e = 0.9$, $\nu_m = \pi/2\sqrt{3}$, $\nu_\mu = 0.71$.

(a) Full model; (b) dense limit.

phase diagrams in the (H, ν)-plane look qualitatively similar (not shown) to those for model-B^p as in figure 6, with the only difference being slightly higher growth rates for the least-stable mode. It is noteworthy that with the global EOS, the flow becomes unstable to shear-banding instabilities at very small values of H for $\nu \geqslant \nu_f$.

From this section, we can conclude that within the framework of a "dense" constitutive model (that incorporates only collisional contributions to transport coefficients, §2.1.2), a simple modification with a global equation of state for *pressure* induces new shear-banding instabilities at large densities; however, a similar modification with a global equation of state for *thermal conductivity* does not induce any new instability.

4.3. *Results for model-C and model-D: influence of viscosity divergence*

As discussed in §2.3, model-C is the same as model-A, with the viscosity divergence being at a lower density $\nu = \nu_\mu < \nu_m$. On the other hand, model-D is the most general model that incorporates the viscosity divergence at a lower density $\nu = \nu_\mu < \nu_m$ (equation 2.23) as well as global equations for pressure (equation 2.17) and thermal conductivity (equation 2.21). The

stability results for these two models are found to be similar, and hence we present results only for model-C.

Figures 7(a) and 7(b) show phase-diagrams in the (H, ν)-plane for model-C and its dense variant model-C_d, respectively; the results are shown up-to the viscosity divergence since uniform shear is not a solution for $\nu > \nu_\mu$. For the full model in figure 7(a), the phase-diagram looks similar to those for model-A and model-B. For its dense counterpart in figure 7(b), the phase-diagram is similar to that for model-B_d and model-B_d^p in the sense that all three models support shear-banding instabilities at large densities. Therefore, for model-C_d, the viscosity divergence induces shear-banding instabilities at large densities. This prediction is in tune with the results of Khain & Meerson (2006) whose model is similar to our model-C_d (see § 5.3).

Within the framework of a "dense" model (§2.1.2), therefore, we can conclude about the emergence of shear-banding instabilities at large densities: (1) a global equation of state for pressure alone can induce shear-banding instabilities; (2) a viscosity-divergence at a density, $\nu = \nu_\mu$, lower than the maximum packing density alone can induce shear-banding instabilities.

5. Discussion: Universality of shear-banding instability and crystallization

5.1. *An universal criterion for shear-banding instability*

Since the shear-banding instability is a *stationary* ($\omega_i = 0$) mode, this instability is given by one of the real roots (equation (3.10)) of the dispersion relation. The condition for neutral stability ($\omega_r = 0$) can be obtained by setting $\omega = 0$ in the dispersion relation (3.8):

$$a_0 = 0 \quad \Rightarrow \quad k_n^2/H^2 = \frac{\Psi_2}{\Psi_1}, \tag{5.1}$$

where

$$\Psi_1 = \frac{f_4}{f_5} \quad \text{and} \quad \Psi_2 = \left(\frac{f_{5\nu}}{f_5} + \frac{f_{2\nu}}{f_2} \right) \frac{f_1}{f_{1\nu}} - 2.$$

For an instability to occur at a given density, there must be a range of 'positive' discrete wave-numbers, i.e., $k_n/H > 0$, which is equivalent to

$$\Psi_2 > 0,$$

since Ψ_1 is always positive. The expression for Ψ_2 can be rearranged to yield (Alam 2006)

$$\frac{\mathrm{d}}{\mathrm{d}\nu}\left(\frac{\sqrt{f_2 f_5}}{f_1}\right) > 0, \qquad (\text{with } f_{1\nu} > 0) \tag{5.2}$$

which must be satisfied for the onset of instability. (It should be noted that (5.2) provides a necessary condition for instability, but the sufficient condition is tied to the thermal-diffusive mechanism that leads to an instability length scale (5.1) which is discussed in §5.2.) The term within the bracket in (5.2) is the ratio between the shear stress, $P_{xy} = \mu\gamma$, and the pressure, p, for the plane Couette flow:

$$\beta_d = \frac{P_{xy}}{p} = \frac{\mu(\frac{\mathrm{d}u}{\mathrm{d}y})}{p} = \frac{f_2\sqrt{T}}{f_1 T} = \frac{f_2}{f_1\sqrt{T}} = \frac{f_2}{f_1\sqrt{f_2/f_5}} \equiv \frac{\sqrt{f_2 f_5}}{f_1}, \tag{5.3}$$

where $\gamma = \mathrm{d}u/\mathrm{d}y$ is the local shear rate (which is a constant for uniform shear flow). This is nothing but the *dynamic friction coefficient* of the shear flow, which must increase with increasing density for the shear-banding instability to occur. Note that as per Navier-Stokes-level description, the steady fully developed plane Couette flow admits solutions for which the shear stress and pressure are constants across the Couette gap. Hence, the dynamic friction coefficient, $\beta_d = \mu(\mathrm{d}u/\mathrm{d}y)/p = \mu\gamma/p$, is a *position-independent* order-parameter for both "uniform" ($\gamma = const.$) and "non-uniform" ($\gamma = \gamma(y)$) shear flows.

For model-A, the variation of β_d with ν is non-monotonic as shown by the solid line in figure 8: in the dilute limit β_d is large whose value decreases with increasing density till a critical density $\nu = \nu_{cr}$ is reached beyond which β_d increases. Recall that the onset of shear-banding instability corresponds to $\frac{d\beta_d}{d\nu} > 0$, denoted by the square-symbol in the inset of figure 8. It is clear from this inset that the full model is unstable to shear-banding instability for $\nu > \nu_{cr}$, the dilute model is unstable at any density (since $\frac{d\beta_d}{d\nu} > 0$ for $\nu > 0$), but the dense model is stable for all densities
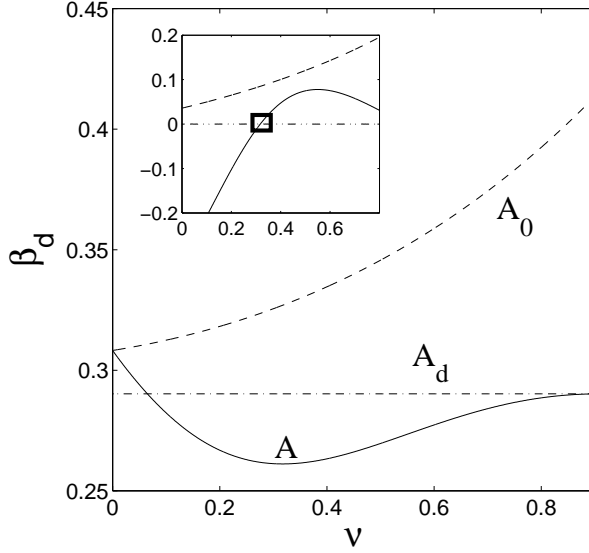
FIGURE 8. Variation of the "dynamic" friction coefficient, $\beta_d = \mu\gamma/p$, with density for model-A: $e = 0.9$, $\nu_m = \pi/2\sqrt{3}$. The inset shows the variation of $\frac{d\beta_d}{d\nu}$ with ν: the onset of shear-banding instability corresponds to $\frac{d\beta_d}{d\nu} > 0$, denoted by the square-symbol.

(since $\frac{d\beta_d}{d\nu} = 0$). It is worth pointing out that, for the full model-A, the critical density for the onset of the shear-banding instability (cf. figure 1) is $\nu_{cr} \approx 0.31733$ which is independent of the restitution coefficient e as confirmed in figure 9. The lower branch of the neutral contour of figure 1 asymptotically approaches this critical density as $H \to \infty$.

For model-B, the variation of β_d with density (ν) is shown in figure 10, and the inset shows the variation of $d\beta_d/d\nu$ with ν. (Recall that this model incorporates the global equations of states for pressure and thermal conductivity.) In contrast to the 'stable' model-A_d, the model-B_d (i.e. the dense variant of model-B) is unstable to shear-banding instabilities for all densities (figure 6b) since $\frac{d\beta_d}{d\nu} > 0$. For the full model-$B$, the critical density for the onset of shear-banding instability (cf. figure 6a) is $\nu_{cr} \approx 0.2351$ which is also independent of the restitution coefficient e (as in figure 9 for model-A). For models C and D, this critical density is $\nu_{cr} \approx 0.2849$ and $\nu_{cr} \approx 0.2207$, respectively.

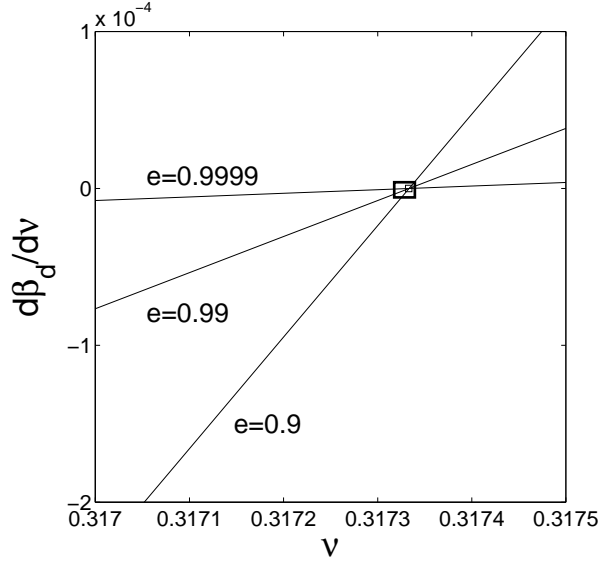It should noted that there is a constraint ($f_{1\nu} > 0$) with our instability criterion (5.2), i.e.,

FIGURE 9. The effect of restitution coefficient e on the variation of $\frac{d\beta_d}{d\nu}$ with ν for model A.
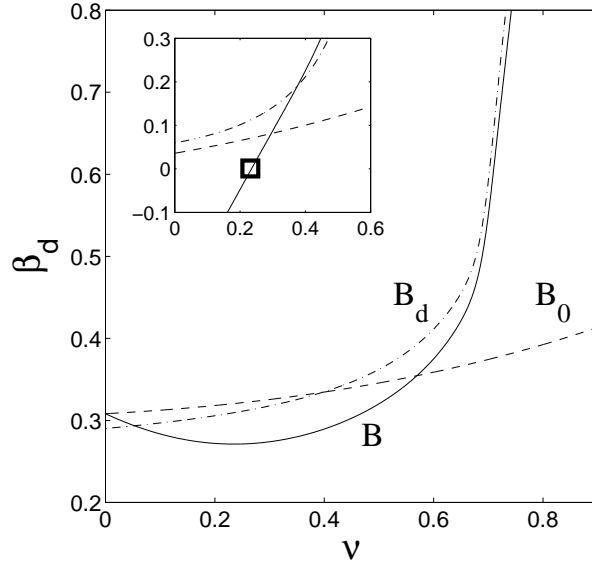

FIGURE 10. Same as figure 8, but for model B.

f_1 should be a monotonically increasing function of density for the instability to occur. This constraint on f_1, see equations (2.7) and (2.19), is satisfied for all four models. The consequence of a possible non-monotonic f_1 is that the shear flow remains stable over a small density range between freezing and melting. However, the increasing dynamic friction with increasing density

(5.2) still remains the criterion for the onset of the shear-banding instability. Even though for an unsheared elastic system, f_1 is non-monotonic (Luding 2001) between freezing and melting density, we retain equation (2.19-2.20) for f_1 since this functional form has been shown to hold up-to the random close-packing density in simulations of plane shear flow of inelastic hard-disks (Volfson *et al.* 2003).

5.1.1. *Shear-banding state and crystallization*

For all four models (A, B, C and D), the shear flow is stable and the system remains homogeneous at low densities, but becomes unstable to shear-banding instability beyond a critical density ($\nu > \nu_{cr}$). This is due to the fact that for $\nu > \nu_{cr}$ the flow cannot sustain the increasing dynamic friction (β_d) and hence breaks into alternating layers of dilute and dense regions along the gradient direction. For $\nu > \nu_{cr}$, the associated "finite-amplitude" bifurcated solution corresponds to a lower shear stress, or, equivalently, a lower dynamic friction coefficient. This has been verified (Alam 2008) numerically by tracking the bifurcated solutions of the associated steady nonlinear equations.

A representative set of such nonlinear bifurcated solutions for the profiles of density $\nu(y)$, granular temperature $T(y)$ and stream-wise velocity $u(y)$ are displayed in figure 11 for three values of the Couette gap $H = 50$, 75 and 125 for model-A; the related numerical procedure is the same as described in Alam *et al.* (2005). For this plot, the mean density is set to 0.5 and the restitution coefficient is 0.9; the corresponding growth-rate variation of the least stable mode can be ascertained from figure $2(a)$. These nonlinear solutions bifurcate from the $n = 1$ mode (see, equations 3.5 and 3.6) of the corresponding linear stability equations, and there is a pair of nonlinear solutions for each H due to the symmetry of the plane Couette flow (Alam & Nott 1998). For mode $n = 1$, the density is maximum at either of the two walls, and this density-maximum approaches the maximum packing density ($\nu_m \approx 0.906$) at $H = 125$ (solid line in figure $11a$) for which we have the coexistence of a "crystalline" zone and a dilute zone, representing a state

of phase separation. Within the crystalline zone, the granular temperature approaches zero (figure 11b) and so does the shear rate (figure 11c). It is noteworthy that the shear-rate is almost uniform and localized within the dilute zone. The resulting two-phase solution is called a "shear-band" (or, shear-localization) since the shearing is confined within a band of an agitated dilute region that coexists with a denser region with negligible shearing (i.e., a crystalline-region at large enough Couette gap).

At $H = 50$ with parameters as in figure 11, there are two possible solutions: a "uniform-shear" state, with the "dynamic" friction coefficient being $\beta_d \approx 0.26965$, which is unstable, and one of two "shear-band" solutions for which $\beta_d \approx 0.2672$. The selection of the stable branch is determined by the value of the dynamic friction coefficient being the lowest among all possible solutions, and therefore the equilibrium state of the flow (at $H = 50$) corresponds to the shear-banding state of a "lower" dynamic friction (Alam 2008).

For higher-order modes ($n = 2, 3, \cdots$), the shape of the nonlinear density/temperature/velocity profiles can be ascertained from (3.5) and (3.6). For example, the density profiles for modes $n = 2$ and 3 would look like the corresponding density eigenfunctions in figure 2(b). In fact, the solution for the first mode ($n = 1$) serves as a "building-block" of solutions for higher modes which has been clarified previously (Alam & Nott 1998; Nott *et al.* 1999; Alam *et al.* 2005).

At this point, we can say that an accurate constitutive model over the whole range of densities (that incorporates both kinetic and collisional modes of transport mechanisms) should be used since the dilute and dense regimes can coexist even at a moderately low mean density. Details of such shear-banding solutions for other models (B, C and D) and their stability as well as the related results from particle-dynamics simulations will be considered in a separate paper. Such an exercise will help to identify and tune the best among the four models.
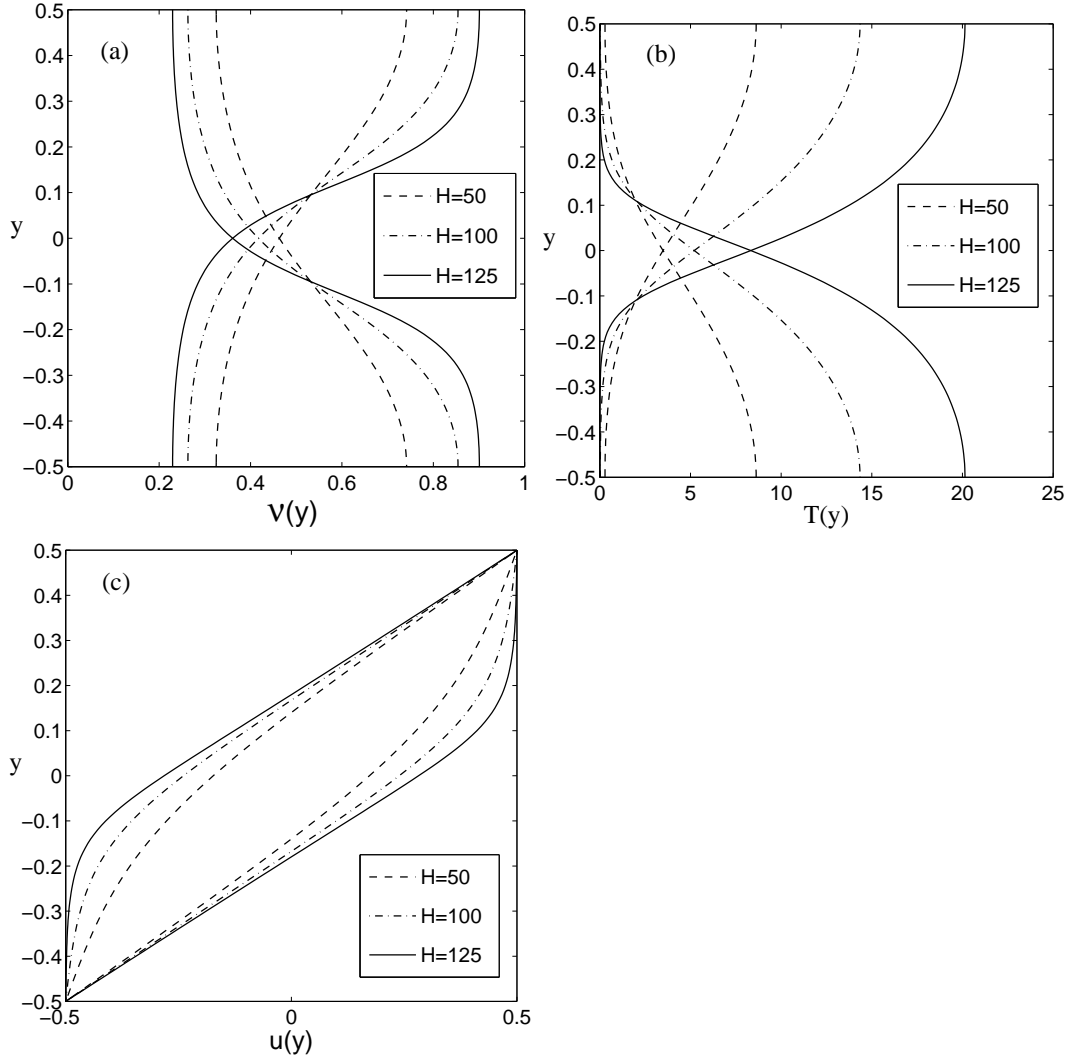
FIGURE 11. Nonlinear shear-banding solutions for model-A for mode $n = 1$ with $\nu = 0.5$ and $e = 0.9$: (a) density, (b) granular temperature and (c) stream-wise velocity.

5.2. *Instability length scale and the effect of dissipation*

While our instability criterion, given by equation (5.2), yields a critical value for the density above which the uniform shear flow is unstable to the shear-banding instability, it does not say anything about the related instability length scale below which the flow is stable (cf. figures 1–7). This issue of a dominant instability length scale is tied to the underlying diffusive mechanisms in a granular fluid, offered by the pseudo-thermal conductivity in the energy balance equation (2.3).

We have mentioned in §4 that the neutral contour in the (H, ν)-plane (such as in figures 1–7)

shifts towards right with increasing restitution coefficient (e), and hence the flow becomes more

stable in the elastic limit. In fact, the dependence of the neutral contour on e can be removed if

we define a normalized Couette gap as

$$H^* = H\sqrt{1 - e^2}, \tag{5.4}$$

which can be thought of as an "instability length scale" (Tan & Goldhirsch 1997; Alam & Nott

1998). This length scale appears directly from an analysis of the equation for the neutral contour

(5.1):

$$H^2/\Psi_1 = k_n^2/\Psi_2 = f_5 H^2/f_4 = f_{50}(1 - e^2)H^2/f_4$$

$$\Rightarrow H\sqrt{1 - e^2} \equiv H^* = k_n \sqrt{\frac{f_4(\nu)}{\Psi_2(\nu) f_{50}(\nu)}}, \tag{5.5}$$

where $f_5(\nu, e) = (1 - e^2)f_{50}(\nu)$, and $f_4(\nu)$ is related to pseudo-thermal conductivity as in (2.6).

This specific functional dependence of the "instability length scale" on the restitution coefficient

is also due to the dependence of the thermal conductivity on the granular temperature which

implicitly depends on e (equation (3.2)): $T \sim f_2/f_5 \sim (1 - e^2)^{-1}$.

In terms of the above instability length scale (5.4), the renormalized stability diagrams in the

(H^*, ν)-plane are displayed in figures 12(a), 12(b), 12(c) for model A, B, C and D, respectively.

In each panel, we have superimposed three neutral contours for $e = 0.9, 0.99$ and 0.999 which are

indistinguishable from each other due to the underlying scaling (5.5) with e. In figure 12(b), we

compared the neutral contour of the full model-B with those for model-B^p (that incorporates the

EOS for pressure) and model-B^κ (that incorporates the global EOS for thermal conductivity). A

global equation for thermal conductivity has little influence on the stability diagram, but a global

equation for pressure significantly enlarges the domain of instability in the (H^*, ν)-plane.

Comparing figure 12(a) with figure 12(b), we find that there is a significant difference be-

tween the predictions of model-A and model-B, especially in the dense limit. In particular, with
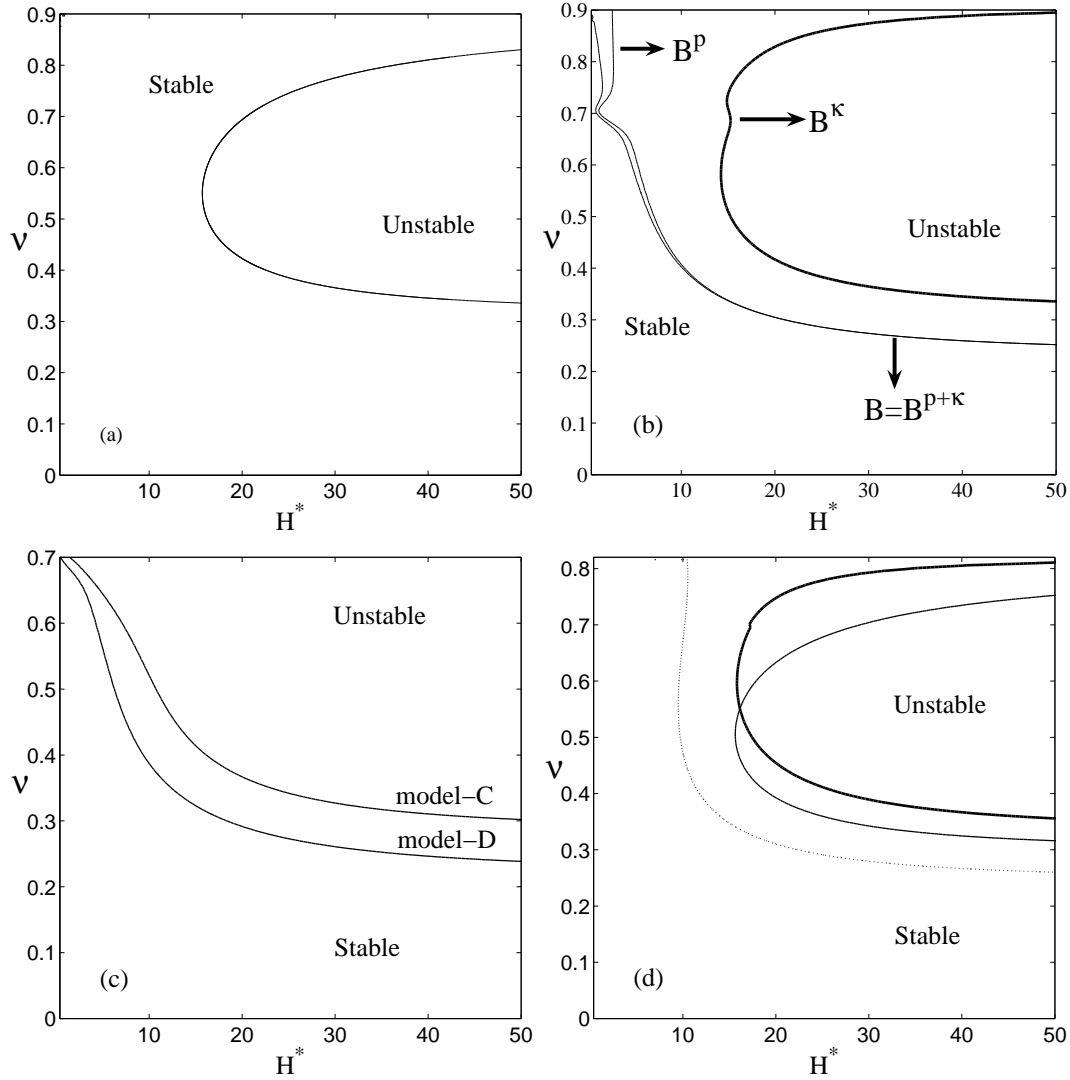
FIGURE 12. Renormalized stability diagrams in the (H^*, ν)-plane, showing the neutral contour that separates stable and unstable regions: (*a*) model A; (*b*) model B; (*c*) model C and D; (*d*) model A with different $\chi(\nu)$ as explained at the end of §5.2. The outermost dotted curve in panel (*d*) is discussed at the end of §5.3. In each panel, the abscissa has been renormalized as $H^* = H\sqrt{1-e^2}$. Note different range of vertical axis in each panel.

accurate equations of state as in model-B, the dense flow is unstable to shear-banding instability even for small values of the Couette gap. This is an important issue beyond the square packing density $\nu > \pi/4$ (in two-dimensions) for which the flow must reorganize internally such that a

part of the flow forms a layered crystalline structure or banding (Alam & Luding 2003), thereby

allowing the material to shear. This reconciles well with the predictions of model-B, but not

with model-A (which uses the standard Enskog expressions for all transport coefficients, §2.1)

for $H^* < 30$ (figure 12a); therefore, using an accurate equation of state over the whole range of

densities should give reasonable predictions for shear-banding solutions.

In this regard, the predictions of model-C (upper curve in figure 12c) and model-D (lower

curve in figure 12c) are also consistent for dense flows since the shear-banding instabilities persist

at small values of H for these models too. It may be recalled that these two models (C and D),

with viscosity divergence at $\nu = \nu_\mu < \nu_m$, do not admit "uniform" shear solution at large

densities $\nu > \nu_\mu$. However, the related shear-banding solutions at $\nu < \nu_\mu$ can be continued to

higher densities $\nu > \nu_\mu$ by embedding the present problem into the uniform shear case such that

the shear work is vanishingly small (Khain & Meerson 2006).

Following one referee's suggestion, we briefly discuss possible effects of Torquato's (1995)

formula for the contact radial distribution function:

$$
\begin{aligned}
\chi(\nu) &= \frac{(1-0.436\nu)}{(1-\nu)^2}, && \text{for} \quad 0 \leqslant \nu \leqslant \nu_f, \\
&= \frac{(1-0.436\nu)}{(1-\nu_f)^2} \frac{(1-\nu_f/\nu_r)}{(1-\nu/\nu_r)}, && \text{for} \quad \nu_f \leqslant \nu \leqslant \nu_r,
\end{aligned}
\tag{5.6}
$$

which is known to be valid for an elastic hard-disk fluid over a range of densities up-to the random

packing limit $\nu_r = 0.82$. When (5.6) is used instead of (2.12) in model-A, the neutral stability

curve in the (H^*, ν)-plane follows the thick line in figure 12(d). For the sake of comparison, we

have also superimposed the neutral stability curve of model-A, denoted by the thin line, with

$\chi(\nu)$ being given by (2.12) with $\nu_m = \nu_r$. Clearly, a larger range in the dense regime is unstable

with Torquato's formula (5.6), but the overall instability characteristics (the stationary nature of

instability, the magnitude of growth rate, etc.) remain similar for both (2.12) and (5.6). We have

also verified that the stability diagram looks similar to that in figure 5 (except for the presence of

a discontinuity on the neutral contour at $\nu = \nu_f$, resulting in two instability lobes) when (2.20)

is used as an effective contact radial distribution function for all transport coefficients.

5.3. *Discussion of some "ultra-dense" constitutive models*

Focussing on the "ultra-dense" regime with volume fractions close to the close-packing density

($\nu \to \nu_m$), the dense limit of model-A (i.e. model A_d in § 2.1.2) can be simplified by replacing ν

with ν_m and retaining the dependence of the f_i's on ν via the corresponding dependence of the

pair correlation function. For this ultra-dense regime the constitutive expressions are:

$$
\begin{aligned}
f_1 &\equiv f_1^c(\nu \to \nu_m) &=& 2\nu_m^2\chi \\
f_2 &\equiv f_2^c(\nu \to \nu_m) &=& \tfrac{\sqrt{\pi}}{8}\left(1 + \tfrac{8}{\pi}\right)\nu_m^2\chi \\
f_3 &\equiv f_3^c(\nu \to \nu_m) &=& \tfrac{2}{\sqrt{\pi}}\nu_m^2\chi \\
f_4 &\equiv f_4^c(\nu \to \nu_m) &=& \sqrt{\pi}\left(\tfrac{1}{\pi} + \tfrac{9}{8}\right)\nu_m^2\chi \\
f_5 &\equiv f_5(\nu \to \nu_m) &=& \tfrac{4}{\sqrt{\pi}}(1 - e^2)\nu_m^2\chi.
\end{aligned}
\tag{5.7}
$$

This model is devoid of shear-banding instabilities since it can be verified that

$$
\frac{\mathrm{d}\beta_d}{\mathrm{d}\nu} = 0, \quad \forall \quad \nu > 0.
$$

This is similar to the predictions of model-A_d (see the dot-dash line in figure 8).

The constitutive model of Khain & Meerson (2006) can be obtained from (5.7) by replacing

the contact radial distribution function for viscosity by

$$
\chi \to \chi^\mu(\nu) = \left(1 + \frac{0.037}{\nu_\mu - \nu}\right)\chi(\nu)
$$

that diverges at $\nu = \nu_\mu$ as in (2.23); the exact density at which viscosity diverges is not important

here. Interestingly, Khain & Meerson found two-phase-type solutions using their model. Since

viscosity diverges at a lower density (and hence "faster") than other transport coefficients, it is

straightforward to verify that our instability criterion,

$$
\frac{\mathrm{d}\beta_d}{\mathrm{d}\nu} > 0, \quad \forall \quad \nu > \nu_{cr},
$$

holds for this model. Recently, Khain (2007) also found two-phase-type solutions using a con-

stitutive model (a modified model of Khain & Meerson 2006) which is similar to our model-D,

and the predictions of his model agree well with particle simulation results; for this modified

model too, our instability criterion (5.2) holds. Therefore, the two-phase-type solutions of Khain

& Meerson (2006, 2007) are directly tied to the shear-banding instabilities of Alam *et al.* (1998,

2005, 2006) via the universal instability criterion (5.2). More specifically, both belong to the

same class of *constitutive instability* (Alam 2006).

The constitutive model of Losert *et al.* (2000) can be obtained from (5.7) by using the follow-

ing functional form for the contact radial distribution function

$$\chi = \left(1 - \nu/\nu_r\right)^{-1},$$

that diverges at the random close packing limit (ν_r), for all transport coefficients except the shear

viscosity, μ, that has a "stronger" rate of increase near ν_r:

$$\chi \to \chi^\mu(\nu) = \left(1 - \nu/\nu_r\right)^{-7/4}.$$

This choice of viscosity satisfies our instability criterion, $\mathrm{d}\beta_d/\mathrm{d}\nu > 0$, and, therefore, the model

of Losert *et al.*would yield shear-banding type solutions which is again tied to the increase of

"dynamic" friction with density for the uniform shear state.

To illustrate the quantitative effect of a stronger viscosity divergence on the shear-banding

instability, the neutral stability contour for model-A (with a stronger viscosity divergence, see

below) is shown in figure 12(d), denoted by the outermost dotted curve. For this case, the con-

stititutive model is the same as the full model-A (i.e. all transport coefficients diverge at the

same density ν_m) but its viscosity function $f_2(\nu)$ in (2.8) is calculated using a radial distribution

function that has a stronger divergence than all other transport coefficients:

$$\chi \to \chi^\mu(\nu) = \frac{1 - 7\nu/16}{(1 - \nu/\nu_m)^q},$$

with its exponent $q = 2.25 > 2$. (It should be noted that this specific functional form of χ^μ may

not be correct quantitatively at all densities, but it has simply been chosen to illustrate the possible effects of a stronger viscosity divergence on instabilities.) Comparing the dotted contour in figure $12(d)$ with the thin-solid contour for model-A, we find that a larger range in the (ν, H^*)-plane is unstable for the case of a stronger viscosity divergence. With further increase of q, the neutral contour shifts towards the left to cover smaller values of H, leading to even larger instability region in the (ν, H^*)-plane. In either case, however, the nature of the shear-banding instability remains the same and we do not find any new instability as emphasized before.

5.4. *Limit of elastic hard-sphere fluid: dissipation versus effective shear rate*

Naively extrapolating the instability length-scale (5.5) to the elastic limit ($e \to 1$) of atomistic fluids results into $H \to \infty$ that corresponds to an infinite system for shear-banding to occur in an atomistic fluid. This is in contrast to molecular dynamics simulations of sheared "elastic" hard-sphere fluid (Erpenbeck 1984) for which a shear-induced ordering phenomenon has been observed at moderate densities (much below the freezing density). Similar observations of such banding have been made in simulations for continuous potentials too (see, Evans & Morriss 1986). The key to resolve this apparent anomaly lies with the fact that the elastic limit ($e = 1$) is singular since the collisional dissipation vanishes. To achieve a steady-state in simulations of a sheared atomistic fluid, thermostats are used to take away energy from the system that compensates the production of energy due to shear-work ($\mathbf{P} : \boldsymbol{\nabla}\mathbf{u}$). Otherwise the system would continually heat up, leading to an infinite temperature. Hence, the collisional dissipation in a granular fluid can be seen to play the role of a thermostat in an atomistic fluid.

Equating the dissipation term (either due to a thermostat in an elastic fluid, or due to inelastic collisions in a granular fluid) with the shear-work, we obtain a scaling relation for temperature with the shear rate and the restitution coefficient:

$$\tilde{T} \quad \propto \quad \frac{\gamma^2}{1 - e^2} \quad \propto \quad \gamma^{*2}, \tag{5.8}$$

where $\tilde{T}$ is the dimensional temperature, and

$$\gamma^* = \frac{\gamma}{\sqrt{1 - e^2}} \qquad (5.9)$$

defined as an "effective" shear rate. For an elastic fluid, this effective shear rate, γ^*, is used to normalize the temperature, and hence a similar criterion (5.2) is likely to hold for the onset of shear-banding instability in an elastic fluid too. The dependence of the effective shear rate (5.9) with inelasticity suggests that the shear-banding in atomistic fluids is likely to occur at large shear rates, a prediction that agrees with Erpenbeck's (1984) simulations. This needs to be checked by determining the analytical expression for the thermostat term (which might depend on the choice of the thermostat) in the energy equation.

While the Erpenbeck's ordering transition has been explained (Kirkpatrik and Nieuwoudt 1986; Lutsko & Dufty 1986) as an instability of the "unbounded" shear flow of an elastic fluid, using Navier-Stokes-level equations with wave-vector-dependent transport coefficients (i.e. generalized hydrodynamics), the latter work by Lee *et al.* (1996) has identified a long-wave instability (with perturbations along the gradient direction only) in the uniform shear flow for all densities. In particular, Lee *et al.* showed that the Navier-Stokes-level constitutive model is the "minimal" model to predict the robustness of this instability. The possible connection of this instability with the present work needs to be investigated in the future.

5.4.1. *Shearbanding criterion in a molecular fluid: Loose and Hess (1989)*

We close our discussion by recalling a similar instability criterion for an "ordering" transition in a dense molecular fluid (Loose and Hess 1989) and its connection (Alam 2006) with our instability criterion (5.2), along with a more general criterion for shear-banding in a shear thinning/thickening fluid.

Using a non-Newtonian constitutive model, Loose and Hess (1989) have derived a criterion

for the onset of shear-banding in a dense molecular fluid:

$$\left(\frac{\partial p_{yx}}{\partial \gamma}\right)\left(\frac{\partial p_{yy}}{\partial \nu}\right) \leqslant \left(\frac{\partial p_{yx}}{\partial \nu}\right)\left(\frac{\partial p_{yy}}{\partial \gamma}\right), \tag{5.10}$$

where p_{yy} and p_{yx} are the normal and shear stresses, respectively. Assuming the following functional dependence of p_{yy} and p_{yx} with density (ν) and shear rate (γ),

$$p_{yy} = p_{yy}^0(\nu)f_{yy}(\gamma) \quad \text{and} \quad p_{yx} = p_{yx}^0(\nu)f_{yx}(\gamma), \tag{5.11}$$

the above instability criterion simplifies to

$$\left(p_{yx}^0 \frac{\mathrm{d}f_{yx}}{\mathrm{d}\gamma}\right)\left(f_{yy}\frac{\mathrm{d}p_{yy}^0}{\mathrm{d}\nu}\right) \leqslant \left(f_{yx}\frac{\mathrm{d}p_{yx}^0}{\mathrm{d}\nu}\right)\left(p_{yy}^0 \frac{\mathrm{d}f_{yy}}{\mathrm{d}\gamma}\right). \tag{5.12}$$

For a granular fluid, the shear-rate dependence of stresses follows the well-known Bagnold scaling:

$$f_{yy}(\gamma) \sim T \sim \gamma^2 \quad \text{and} \quad f_{yx}(\gamma) \sim \gamma\sqrt{T} \sim \gamma^2, \tag{5.13}$$

where we have used the relation of the granular temperature with the shear rate, $T \sim \gamma^2$. Substituting (5.13) into (5.12), the Loose-Hess instability criterion boils down to (Alam 2006)

$$\frac{\mathrm{d}}{\mathrm{d}\nu}\left(\frac{p_{yx}^0}{p_{yy}^0}\right) \geqslant 0. \tag{5.14}$$

The term within the bracket is the dynamic friction coefficient of a fluid, and hence the onset of instability is again tied to the increasing value of this dynamic friction coefficient with increasing density. This is same as our shear-banding instability criterion (5.3). For a more general case, the shear-rate dependence of stresses can be postulated as

$$\begin{aligned} f_{yy}(\gamma) &= \gamma^{2n} \\ f_{yx}(\gamma) &= \gamma^{n+1}, \end{aligned} \tag{5.15}$$

where the index n is a measure of shear-thickening ($n > 0$) or shear-thinning ($n < 0$) behaviour of the fluid. With this, the shear-banding instability criterion boils down to

$$p_{yx}^0 \frac{\mathrm{d}p_{yy}^0}{\mathrm{d}\nu} \leqslant \left(\frac{2n}{n+1}\right) p_{yy}^0 \frac{\mathrm{d}p_{yx}^0}{\mathrm{d}\nu}. \tag{5.16}$$

6. Conclusion and Outlook

To conclude, we showed that by just knowing the constitutive expressions for pressure and shear viscosity, one can determine whether any Navier-Stokes'-level constitutive model would lead to a shear-banding instability in granular plane Couette flow. The onset of this stationary instability is tied to the increasing value of the "dynamic" friction coefficient, $\beta_d = \mu\gamma/p$ (where μ, p and $\gamma = \mathrm{d}u/\mathrm{d}y$ are the shear viscosity, pressure and shear rate, respectively), with increasing density for $\nu > \nu_{cr}$ (equation (5.2)): the "homogeneous" shear flow breaks into alternating layers of dilute and dense regions along the gradient direction since the flow cannot accommodate the increasing friction to stay in the homogeneous state. For $\nu > \nu_{cr}$, the associated "nonlinear" shear-band solution corresponds to a lower shear stress, or, equivalently, a lower dynamic friction coefficient (Alam 2008). In other words, the sheared granular flow evolves toward a state of "lower" dynamic friction, leading to shear-induced band formation along the gradient direction. Note that the dynamic friction coefficient, $\beta_d = \mu\gamma/p$, is a position-independent order-parameter for both "uniform" ($\gamma = const.$) and "non-uniform" ($\gamma = \gamma(y)$) shear flows.

In the framework of a "dense" constitutive model that incorporates only collisional transport mechanism (i.e. Haff's model, 1983), we showed that an accurate global equation of state for pressure or a viscosity divergence at a lower density (with other transport coefficients being given by respective Enskog values) can induce shear-banding instabilities, even though the original dense Enskog model is stable to such shear-banding instabilities. Since the prediction of the shear-banding instability depends crucially on the form of the constitutive relations, we need to use accurate forms of constitutive expressions over the whole range of density that incorporate both kinetic and collisional transport mechanisms. The latter statement is important since the dilute and dense regimes coexist even at a low mean density when the uniform shear flow is unstable to shear-banding instability. The resulting nonlinear shear-banding solutions of all four models (A, B, C and D) and their stability as well as the related results from particle-dynamics

simulations will be considered in a separate paper. This will help to identify the best among these four constitutive models, or will point towards new models. In this regard, it is recommended that the particle-dynamics simulations be used to find out accurate expressions (valid over the whole range of density) for all transport coefficients.

We established that the two-phase-type solutions of Khain & Meerson (2006) are directly related to the shear-banding instabilities of Alam *et al.* (1998, 2005, 2006) via the universal instability criterion (5.2), and both belong to the same class of *constitutive instability* (Alam 2006). In particular, the instabilities arising out of non-monotonicities of constitutive relations with mean-fields (e.g. the coil-stretch transition is tied to non-monotonic stress-strain curve; see, de Gennes 1974) are of constitutive origin and hence dubbed constitutive instability. The same universal criterion (5.2) also holds for the constitutive model of Losert *et al.* (2000), thereby yielding such two-phase-type solutions in their model of plane shear flow.

The onset of the ordering transition of Erpenbeck (1984) in a sheared "elastic" hard-sphere fluid (which is close to our granular system) is accompanied by a decrease in viscosity and hence a lower viscous dissipation. Therefore, similar to the sheared granular fluid, the state of lower viscosity/friction is the preferred equilibrium state for a sheared atomistic fluid. Our instability criterion (5.2) seems to provide a unified description for the shear-banding phenomena for the singular case of hard-sphere fluids if we relate the collisional dissipation to a thermostat, leading to an "effective" shear rate. This possible connection needs to be investigated further from the viewpoint of a constitutive instability of the underlying field equations.

The shear-banding phenomenon is ubiquitous in a variety of complex fluids under non-equilibrium conditions: wormlike micelles (Spenley, Cates & McLeish 1993), colloidal suspensions (Hoffman 1972; Ackerson & Clark 1984), model glassy material (Varnik *et al.* 2003), suspensions of rod-like viruses (Lettinga & Dhont 2004), lyotropic liquid crystals (Olmsted 2008) and numerous other systems. In the literature of non-Newtonian fluids (see, for a review, Olmsted 2008), the

shear-banding phenomenon has been explained as a constitutive instability from the linear stability analysis of appropriate constitutive models (Greco & Ball 1997; Wilson & Fielding 2005). The well-known "Hoffman-transition" in a colloidal suspension (banding/ordering of particles along the gradient direction) above the freezing density is accompanied by a sharp decrease in viscosity and has been explained in terms of a flow-instability (Hoffman 1972). A very recent work (Caserta, Simeone & Guido 2008) on biphasic liquid-liquid systems showed that the shear-induced banding in such systems is tied to a lower viscosity, or, equivalently, a lower viscous dissipation. For both cases, the criterion of lower viscosity is similar to our criterion of a lower "dynamic" friction for the band-state in sheared granular fluid. It appears that the shear-induced banding in many complex fluids has a common theoretical description in terms of "constitutive" instability that leads to an ordered-state of a lower viscosity/friction.

REFERENCES

ACKERSON, B. J. & CLARK, N. A. 1984 Shear-induced partial translational ordering of a colloidal solid. *Phys. Rev. A* **30**, 906.

ALAM, M. 2005 Universal unfolding of pitchfork bifurcations and the shear-band formation in rapid granular Couette flow. In *Trends in Applications of Mathematics to Mechanics* (ed. Y. Wang & K. Hutter), pp. 11-20, Shaker-Verlag, Aachen.

ALAM, M. 2006 Streamwise structures and density patterns in rapid granular Couette flow: a linear stability analysis. *J. Fluid Mech.* **5**53, 1.

ALAM, M. 2008 Dynamics of sheared granular fluid. In *Proc. of 12th Asian Congress of Fluid Mechanics* (ed. H.J. Sung), pp. 1-6, 18–21 August, Daejeon, Korea.

ALAM, M., ARAKERI, V., GODDARD, D., NOTT, P. & HERRMANN, H. 2005 Instability-induced ordering, universal unfolding and the role of gravity in granular Couette flow. *J. Fluid Mech.* **5**23, 277.

ALAM, M. & LUDING, S. 2003a Rheology of bidisperse granular mixture via event-driven simulations. *J. Fluid Mech.* **4**76, 69.

ALAM, M. & LUDING, S. 2003 First normal stress difference and crystallization in a dense sheared granular fluid. *Phys. Fluids* **15**, 2298.

ALAM, M. & LUDING, S. 2005 Energy noequipartition, rheology and microstructure in sheared bidisperse granular mixtures. *Phys. Fluids* **17**, 063303.

ALAM, M. & NOTT, P. R. 1998 Stability of plane Couette flow of a granular material. *J. Fluid Mech.* **377**, 99.

ALAM, M. & NOTT, P. R. 1997 Influence of friction on the stability of unbounded granular shear flow. *J. Fluid Mech.* **343**, 267.

CAMPBELL, C. S. 1990 Rapid granular flows. *Annu. Rev. Fluid Mech.* **22**, 57.

CASERTA, S., SIMEON, M. & GUIDO, S. 2008 Shearbanding in biphasic liquid-liquid systems. *Phys. Rev. Lett.* **100**, 137801.

CONWAY, S. & GLASSER, B. J. 2004 Density waves and coherent structures in granular Couette flow. *Phys. Fluids* **16**, 509.

DE GENNES, P. G. 1974 Coil-stretch transition of dilute flexible polymers under ultra-high gradients. *J. Chem. Phys.* **60**, 5030.

ERPENBECK, J. 1984 Shear viscosity of the hard sphere fluid via non-equilibrium molecular dynamics. *Phys. Rev. Lett.* **52**, 1333.

EVANS, D. J. & MORRISS, G. P. 1986 Shear thickening and turbulence in simple fluids. *Phys. Rev. Lett.* **56**, 2172.

GARCIA-ROJO, R., LUDING, S. & BREY, J. J. 2006 Transport coefficients for dense hard-disk systems. *Phys. Rev. E* **74**, 061305.

GASS, D. M. 1971 Enskog theory for a rigid disk fluid. *J. Chem. Phys.* **54**, 1898.

GAYEN, B. & ALAM, M. 2006 Algebraic and exponential instabilities in a sheared micropolar granular fluid. *J. Fluid Mech.* **567**, 195.

GAYEN, B. & ALAM, M. 2008 Orientational correlation and velocity distributions in uniform shear flow of a dilute granular gas. *Phys. Rev. Lett.* **100**, 068002.

GRECO, F. & BALL, R. C. 1997 Shear-band formation in a non-Newtonian fluid model with a constitutive instability. *J. Non-Newt. Fluid Mech.* **69**, 195.

GOLDHIRSCH, I. 2003 Rapid granular flows. *Annu. Rev. Fluid Mech.* **35**, 267.

HAFF, P. K. 1983 Grain flow as a fluid-mechanical phenomenon. *J. Fluid Mech.* **134**, 401.

HENDERSON, D. 1975 A simple equation of state for hard discs. *Mol. Phys.* **30**, 971.

HOPKINS, M. & LOUGE, M. Y. 1991 Inelastic microstructure in rapid granular flows of smooth disks. *Phys. Fluids A* **3**, 47.

HOFFMAN, R. L. 1972 Discontinuous and dilatant viscosity behaviour in concentrated suspensions. I. Observation of a flow instability. *Trans. Soc. Rheol.*, **16**, 155.

JENKINS, J. T. & RICHMAN, M. W. 1985 Kinetic theory for plane flows of a dense gas of identical, rough, inelastic, circular disks. *Phys. Fluids* **28**, 3485.

KIRKPATRICK, T. R. & NIEUWOUDT, J. C. 1986 Stability analysis of a dense hard-sphere fluid subjected to large shear-induced ordering. *Phys. Rev. Lett.* **56**, 885.

KHAIN, E. 2007 Hydrodynamics of fluid-solid coexistence in dense shear granular flow. *Phys. Rev. E* **75**, 051310.

KHAIN, E. & MEERSON, B. 2006 Shear-induced crystallization of a dense rapid granular flow: Hydrodynamics beyond the melting point. *Phys. Rev. E* **73**, 061301.

LEE, M., DUFTY, J. W., MONTANERO, J. M., SANTOS, A. & LUTSKO, J. F. 1996 Long wavelength instability for uniform shear flow. *Phys. Rev. Lett.* **76**, 2702.

LETTINGA, M. P. & DHONT, J. K. G. 2004 Non-equilibrium phase behaviour of rodlike viruses under shear flow. *J. Phys. Cond. Matter* **16**, S3929.

LOOSE, W. & HESS, S. 1989 Rheology of dense model fluids via nonequilibrium molecular dynamics: shear-thinning and ordering transition. *Rheol. Acta* **28**, 101.

LOSERT, W., BOCQUET, L., LUBENSKY, T. C. & GOLLUB, J. P. 2000 Particle dynamics in sheared granular matter. *Phys. Rev. Lett.* **85**, 1428.

LUDING, S. 2001 Global equation of state of two-dimensional hard-sphere systems. *Phys. Rev. E* **63**, 042201.

LUDING, S. 2002 Liquid-solid transition in bidisperse granulates. *Adv. Complex Syst.* **4**, 379.

LUDING, S. 2008 From dilute to very dense granular media. *In preparation*.

LUN, C. K. K., SAVAGE, S. B., JEFFREY, D. J. & CHEPURNIY, N. 1984 Kinetic theories for granular flow: inelastic particles in Couette flow and slightly inelastic particles in a general flow field. *J. Fluid Mech.* **140**, 223.

LUTSKO, J. F. & DUFTY, J. W. 1986 Possible instability for shear-induced order-disorder transition. *Phys. Rev. Lett.* **57**, 2775.

MCNAMARA, S. 1993 Hydrodynamic modes of a uniform granular medium. *Phys. Fluids A* **5**, 3056.

MUETH, D. M., DEBREGEAS, G. F., KARCZMAR, G. S., ENG, P. J., NAGEL, S. & JAEGER, H. J. 2000 Signatures of granular microstructure in dense shear flows. *Nature* **406**, 385.

NOTT, P. R., ALAM, M., AGRAWAL, K., JACKSON, R. & SUNDARESAN, S. 1999 The effect of boundaries on the plane Couette flow of granular materials: a bifurcation analysis. *J. Fluid Mech.* **3**97, 203.

OLMSTED, P. D. 2008 Perspective on shear banding in complex fluids. *Rheol. Acta* **47**, 283.

SAITOH, K. & HAYAKAWA, H. 2007 Rheology of a granular gas under a plane shear. *Phys. Rev. E* **75**, 021302.

SAVAGE, S. B. & SAYED, S. 1984 Stresses developed by dry cohesionless granular materials sheared in an annular shear cell. *J. Fluid Mech.* **142**, 391.

SELA, N. & GOLDHIRSCH, I. 1998 Hydrodynamic equations for rapid shear flows of smooth, inelastic spheres, to Burnett order. *J. Fluid Mech.* **361**, 41.

SHUKLA, P. & ALAM, M. 2008 Nonlinear stability of granular shear flow: Landau equation, shearbanding and universality. In *Proc. of International Conference on Theoretical and Applied Mechanics* (ISBN 978-0-9805142-0-9), 24–29 August, Adelaide, Australia.

SPENLEY, N. A., CATES, M. E. & MCLEISH, T. C. B. 1993 Nonlinear rheology of wormlike micelles. *Phys. Rev. Lett.* **71**, 939.

TAN, M. & GOLDHIRSCH, I. 1997 Intercluster interactions in rapid granular shear flows. *Phys. Fluids* **9**, 856.

TORQUATO, S. 1995 Nearest-neighbour statistics for packings of hard spheres and disks. *Phys. Rev. E* **51**, 3170.

TSAI, J. C., VOTH, G. A. & GOLLUB, J. P. 2003 Internal Granular dynamics, shear-induced crystallization, and compaction steps. *Phys. Rev. Lett.* **91**, 064301.

VARNIK, F., BOCQUET, L., BARRAT, J.-L. & BERTHIER, L. 2003 Shear localization in model glass. *Phys. Rev. Lett.* **90**, 095702.

VOLFSON, D., TSIMRING L. S. & ARANSON, I. S. 2003 Partially fluidized shear granular flows: Continuum theory and molecular dynamics simulations. *Phys. Rev. E* **68**, 021301.

M. Alam, P. Shukla and S. Luding

WILSON, H. J. & FIELDING, S. M. 2005 Linear instability of planer shear banded flow of both diffusive and non-diffusive Johnson-Segelman fluids. *J. Non-Newt. Fluid Mech.* **138**, 181.